PHYSICAL REVIEW B **89**, 115436 (2014)

Understanding surface core-level shifts using the Auger parameter: A study of Pd atoms adsorbed on ultrathin SiO_2 films

William E. Kaden,* Christin Büchner, Leonid Lichtenstein, Stefanie Stuckenholz, Franziska Ringleb, Markus Heyde, Martin Sterrer, and Hans-Joachim Freund
Department of Chemical Physics, Fritz Haber Institute of the Max Planck Society, Faradayweg 4-6 D-14195 Berlin, Germany

Livia Giordano and Gianfranco Pacchioni
Dipartimento di Scienza dei Materiali, Università di Milano-Bicocca, Via Cozzi 53, I-20125 Milano, Italy

Connie J. Nelin and Paul S. Bagus
Department of Chemistry, University of North Texas, Denton, Texas 76203-5017, USA
(Received 31 July 2013; revised manuscript received 23 January 2014; published 27 March 2014)

Auger parameter ($\Delta\alpha$) measurements have been employed to determine the extent to which initial- and final-state effects govern surface core-level shifts in x-ray photoelectron spectroscopy (XPS) measurements of Pd atoms confined between a bilayer SiO_2 film and its Ru(0001) support. For atoms bound in this manner, we note negative binding energy shifts (ΔBEs) of $\sim$0.3 eV, relative to the Pd 3*d* peak position in the bulk, and attribute these shifts to large variations in the initial-state orbital energies of the supported atoms ($\sim$1.1 eV towards E_F), coupled with decreased final-state relaxation contributions ($\sim$0.8 eV). Theoretical calculations reveal that, despite small partial positive charges and decreased final-state screening, the decreased 4*d*-5*sp* hybridization of the undercoordinated Pd atoms results in large enough upward 3*d* orbital-energy shifts to yield the net-negative ΔBE noted by XPS.

DOI: 10.1103/PhysRevB.89.115436 PACS number(s): 82.80.Ej, 31.15.A−, 71.15.Mb, 73.20.−r

I. INTRODUCTION

Thirty-five years ago, initial x-ray photoelectron spectroscopy (XPS) studies of surface core-level shifts (SCSs) provided the first unambiguous empirical differentiation of electron binding energies (BEs) associated with photoemission from surface versus bulk atoms in Au and W samples [1,2]. Since that time, much work has gone into developing a fundamental understanding of the physical phenomena governing such effects [3–5], and while most agree that narrowing of the *d* band due to decreasing atomic coordination plays a crucial role in determining the SCS for metals, there has been considerable debate regarding the extent to which the ΔBEs reflect the resultant changes to either the initial- or final-state configurations of the photoemission processes [4,6], and disentanglement of these contributions becomes even more difficult when evaluating XPS shifts associated with supported metals, as a number of effects, such as charge transfer, lattice contraction [7], electrostatic charging [8], size-dependent final-state screening [9], and variation of the reference level, relative to bulk [4], also become important factors.

To address this issue empirically, Wagner established the Auger parameter (α) [10], which consists of the difference between the kinetic energies (KEs) of XPS and Auger peaks from the same atom in a given material [11]. Due to the inverse relationship between BE and KE, and the arbitrary nature of the absolute value of α, which is dependent on the photon energy of the excitation source, one can just as easily describe this number as the sum of the XPS BE and the Auger transition KE; a fact that has been pointed out by Wagner and Taylor and employed by others [12,13]. Using only simple math and a few approximations, the change noted in this value ($\Delta\alpha$) when comparing the same spectra for a given atom in different environments has been shown to relate to changes exclusively in the final state of core-level photoemission processes via the following equation:

$$\Delta\alpha = \Delta(\mathrm{BE_{XPS}} + \mathrm{KE_{Auger}}) = 2\Delta R, \tag{1}$$

where R is defined as the relaxation contribution to the final state of a core-level BE. In the most simplistic view, the derivation of Eq. (1) presumes the following relationships:

$$\Delta E_B(i) = -\Delta\varepsilon_i - \Delta R_i, \tag{2}$$

$$\Delta E_{\mathrm{Kin}}(jkk) = -\Delta\varepsilon_j - \Delta R_j + 2\Delta\varepsilon_k + \Delta R_{kk}, \tag{3}$$

$$\Delta R_{kk} = 4\Delta R_k, \tag{4}$$

$$\Delta\varepsilon_i = \Delta\varepsilon_j = \Delta\varepsilon_k, \tag{5}$$

$$\Delta R_i = \Delta R_j = \Delta R_k, \tag{6}$$

where ε_i is the ground-state orbital energy of an electron in the ith level prior to photoemission, R_i represents the total energy associated with full relaxation of a final state with an electron hole in the ith level, $E_B(i)$ is the BE of an electron in the ith orbital, and $E_{\mathrm{Kin}}(jkk)$ is the KE of an Auger electron ejected from the kth orbital upon relaxation of a secondary k electron into a previously created core hole in the jth level. As can be seen from the definition of $\Delta E_B(i)$, we have opted to follow the convention of assigning negative values to orbital energies, such that negative changes to $\Delta\varepsilon_i$ result in positive BE shifts and vice versa. By the same token, we note that decreases in the amount of final-state relaxation (negative ΔR_i) also

*kaden@fhi-berlin.mpg.de

result in larger BEs (smaller KEs), as would be expected from basic-level understandings of photoemission processes.

A central assumption of this general approach is that $\Delta\text{BE}\,(-\Delta\varepsilon_n - \Delta R_n)$ will be equal for all electrons, regardless of orbital. This, however, is empirically false [14], especially when comparing changes in valence and deeper core levels [15], which many continue to do by incorporating easily accessed core-valence-valence Auger measurements into their $\Delta\alpha$ experiments. To circumvent this problem associated with the original definition put forth by Wagner, a modified Auger parameter (β) was created [13] in which the following (more specific) relationship was proposed:

$$\Delta\beta = \Delta[2E_B(i) - E_B(j) + E_{\text{Kin}}(jii)] = 2\Delta R_i. \quad (7)$$

In this case β represents a combination of three experimentally measured values that are chosen in a way that no longer requires the assumptions made in Eqs. (5) and (6). When measurement of the full $\Delta\beta$ is not experimentally practical, the following modified version of the term can also be used:

$$\Delta\beta = \Delta E_B(i) + \Delta E_{\text{Kin}}(jii) = 2\Delta R_i. \quad (8)$$

This modified $\Delta\beta$ is essentially a very specific form of the original $\Delta\alpha$, where the Auger measurement is limited to core-core-core lines with final states consisting of two holes in the same orbital probed by the XPS measurement. By constraining the nature of the Auger line that may be used in the modified $\Delta\beta$ analysis, the impact of the assumptions made in Eqs. (5) and (6) is greatly reduced relative to its potential to affect the more generic $\Delta\alpha$ measurements. As a result, both theoretical and experimental investigations into the validity of the modified term have shown it to provide an accurate separation of initial- and final-state shifts, with results comparable to those obtained from unmodified $\Delta\beta$ measurements [13,15]. For the reasons already specified, the same cannot be said for poorly chosen $\Delta\alpha$ combinations following Wagner's less-constrained original formalism [15].

In the interest of better understanding the driving forces governing SCSs, we have compared the results from such a $\Delta\beta$ analysis with those from theoretical calculations for a model system prepared in a manner that results in the segregated binding of isolated metal atoms at the interface of a dissimilar metal; thereby creating samples with large concentrations of inherent surface species, without complicating contributions from nonsurface moieties, which are typically present in bulk metals and supported clusters. To achieve this, we have made use of a Pd/SiO_2/Ru system, for which scanning-tunneling microscopy (STM) and density functional theory (DFT) results suggest a preference for the adsorption of atomically isolated Pd atoms at the interface between the oxide film and its metallic support. By studying the electronic properties of such samples, we hope to (i) improve upon the current understanding of the fundamental effects governing SCSs by utilizing modified $\Delta\beta$ measurements to *experimentally* deconvolute initial- and final-state contributions to the net changes in measured Pd $3d$ ΔBEs, and (ii) make use of comparison with theoretical calculations to corroborate and extend upon our $\Delta\beta$-based conclusions.

II. EXPERIMENTAL METHODS

Experiments for this work were conducted within two ultrahigh vacuum (UHV) chambers. In both cases, bilayer SiO_2 films were grown over Ru(0001) single-crystal surfaces, which were first cleaned via several Ar^+ sputtering and UHV annealing cycles. The film, which has been the subject of a number of previous studies [16–18], can be described as a honeycomblike sheet physisorbed over O-covered Ru and was grown by evaporating $\sim 1.6 \times 10^{15}$ atoms/cm^2 Si onto the samples within an oxygen environment ($\sim 1.5 \times 10^{-7}$ Torr O_2) at $T \leq 300$ K, heating to $T \approx 1200$ K within $\sim 2 \times 10^{-6}$ Torr O_2, and then cooling the sample before evacuating the O_2. As discussed elsewhere [16,19], both cooling rate and Si coverage can play a role in determining the crystallinity of the film, and the samples created for this work always exhibited a combination of coexisting two-dimensionally amorphous and crystalline phases.

In the first setup, which was used to obtain STM data, films were first examined with low energy electron diffraction (LEED) and Auger electron spectroscopy (AES, combined four-grid optics from Specs) before introduction into the custom-built, dual-mode STM and noncontact atomic force microscopy (nc-AFM) chamber to ensure film quality and cleanliness before imaging the samples. Within the microscope, small amounts of Pd were deposited onto the sample at $\sim$5 K using a custom-built microevaporator positioned near the sample [20]. The resultant Pd coverages were then estimated from the frequency of the Pd features within several images of varying dimensions across the sample.

In the second setup, which was used for the modified $\Delta\beta$ measurements, film growth was characterized by a combination of LEED (Specs), XPS (Al K_α, Specs), and low-energy helium ion scattering spectroscopy (ISS; dual-mode hemispherical analyzer, Specs) in a manner similar to that described elsewhere [16]. After film growth, controlled amounts of Pd were evaporated onto the SiO_2/Ru(0001) at $T \approx 150$ K, and the sample was subsequently kept below this temperature for the full duration of the ensuing XPS and Auger electron measurements. The absolute Pd concentration was calibrated using comparisons to $3d$ XPS data recorded from Pd(111), for which NIST effective attenuation length calculations were applied to account for the depth-dependent loss of the photoemission signal [21]. Concentrations obtained in this manner show good agreement ($\pm$10%) with values predicted from quartz microbalance measurements made prior to deposition.

As the energy needed to excite the $L_3M_{45}M_{45}$ Pd transition ($h\nu > 3200$ eV) [22] exceeds that of our light source (Al $K_\alpha = 1486.6$ eV), we relied on the inherent Bremsstrahlung radiation to probe the Auger peak. As the functional range of our hemispherical analyzer extends up to 3 kV, measurement of the Auger transition (e^- KE $\approx$ 2470 eV) was relatively straightforward, but interpretation of the results was somewhat complicated by the presence of weak Auger features related to the Ru(0001) support that appear in the same energy range. To remove these background contributions, the Auger data presented below represents a subtraction of the signal measured from the uncovered SiO_2/Ru sample from the Pd/SiO_2/Ru one. To ensure the proper function of the hemispherical analyzer under these atypical conditions, analogous data was also

collected with the sample sufficiently biased to shift the e^- KE of this peak (relative to ground) into the range of energies normally probed during XPS, and the results of this experiment confirmed the findings from the unbiased sample. Finally, reference measurements of both the $3d$ and $L_3M_{45}M_{45}$ lines were also recorded from a freshly cleaned Pd(111) sample to facilitate the chemical-state discussions that follow below.

III. COMPUTATIONAL METHODS

A. DFT supercell calculations

Density functional theory calculations were carried out with a periodic approach and plane wave basis set, as implemented in the VASP code [23,24]. We explicitly treated four valence electrons for Si ($3s^23p^2$), six for O ($2s^22p^4$), eight for Ru ($4d^75s^1$), and ten for Pd ($4d^{10}$). Core electrons were described with the projector augmented wave (PAW) method [25], and the plane wave cutoff was set to 400 eV. The gradient-corrected PBE [26] functional has been employed, and we have included an estimate of the van der Waals interactions, with the pairwise force field implemented in the DFT-D2 method proposed by Grimme [27].

The SiO_2 film has been modeled by considering the hexagonal bilayer adsorbed on the oxygen covered Ru(0001) surface [3O-(2 × 2)/Ru(0001) structure]. The metal surface was modeled by a five-layer thick slab at the optimized bulk Ru lattice parameters. The slabs were separated by 12 Å of vacuum and a dipole correction has been added in order to eliminate the interaction between repeated replicas. For the adsorption of isolated metal atoms, a (2 × 2) SiO_2 supercell was employed, with a (3 × 3 × 1) Monkhorst-Pack grid. The positions of Pd adatom, SiO_2, and the two Ru upper layers were relaxed until the forces were smaller than 0.01 eV/Å^3. Atomic charges have been obtained within the scheme of charge density decomposition proposed by Bader [28].

The core-level binding energies have been computed in both initial-state approximation and final-state effects. In initial-state calculations, after a full self-consistency with frozen core electrons is achieved, the Kohn-Sham equations are solved for core electrons inside the PAW sphere, and the core-level shift (CLS) is computed as the difference of the resulting Kohn-Sham eigenvalues (referred to the Fermi level). In final state calculations, excitation of a single core electron is accounted for by the corresponding core-excited ionic PAW potential. Due to the frozen core, this method accounts for screening by valence electrons but neglects screening by core electrons, which is justified by the fact that the latter term is practically constant. Within this approach, core-level binding energy shifts can be computed as total energy differences [29]. For these calculations we have constructed a model where five Pd(111) layers have been added below the SiO_2/3O-(2 × 2)/Ru(0001–3 ML) film, so that the isolated adatom and the fully coordinated (bulk) reference Pd atoms are in the same unit cell and their core-level binding energies can be directly compared.

B. HF cluster calculations

Hartree-Fock (HF) wave functions were calculated for initial and final states of a Pd_{13} cluster to model BE shifts for bulk Pd, a Ru_9Pd cluster used to simulate Pd adsorbed at an open threefold site on Ru(0001), and an isolated Pd atom; Pd_{13} and Ru_9Pd are shown schematically in Fig. 1. The Pd_{13} cluster contains a central Pd atom with its 12 nearest neighbors in the fcc geometry of Pd at bond distances consistent with the bulk Pd lattice constant. Likewise, the Ru_9 substrate has bond distances equivalent to those in hcp Ru [30]. The distance between the Pd atom and the Ru surface was taken from the results of the DFT calculations described above. The wave functions are nonrelativistic and spin-orbit splitting is not included; for the open shell configurations, the energies and orbitals were optimized for the average of configurations [31]. For these systems, several states are considered. These are: the ground state and core-hole states, where a $3d$ electron is removed, a $2p$ electron is removed, and where two electrons are removed from the $3d$ shell. The core-ionized Pd atom in the Pd_{13} cluster is the central atom. The single-hole states are used to calculate BE($2p$) and BE($3d$); the double hole state is used to describe the final state of the *LMM* Auger transition. For the core-hole configurations, the energy is computed with ground-state frozen orbitals (FOs) and with orbitals optimized for the core-hole configurations (ΔSCF) [32]. With these states we are able to compute relaxation energies E_R for the single- and double-hole configurations, FO or Koopmans' theorem (KT), BEs [denoted BE(KT)], and fully relaxed BEs [denoted BE(ΔSCF)]; see Ref. [32] for definitions of these initial- and final-state quantities. All the electrons of the core-ionized Pd are explicitly included in the calculation so that the Pd core BEs can be directly calculated; for the other atoms in the clusters a pseudo or effective core potential (ECP) is used. The ECP parameters and basis sets for these atoms are from the work of Hay *et al*. [33]. The all electron basis set for Pd was modified from the set given in Ref. [34].

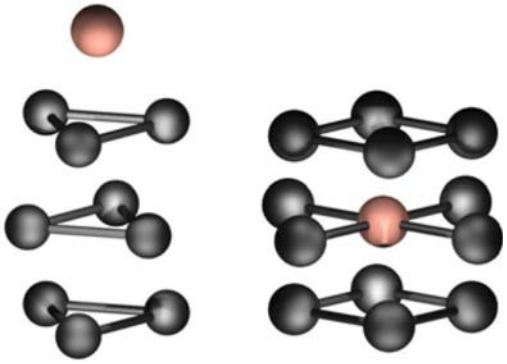

FIG. 1. (Color online) Depictions of the Pd/Ru_9 (left) and Pd_{13} (right) clusters are provided with the Pd atoms used for the ΔBE(ΔSCF) calculations highlighted in both cases.

IV. RESULTS AND DISCUSSION

Highlighted in Fig. 2 are STM and DFT results from our initial investigations into the structure of the Pd/SiO_2/Ru system, which will be the main subject of a forthcoming publication [35]. Included in this figure are a low-temperature STM image collected after depositing a small concentration (<5 × 10^{12} atoms/cm^2) of Pd over the film at ∼5 K [Fig. 2(a)]

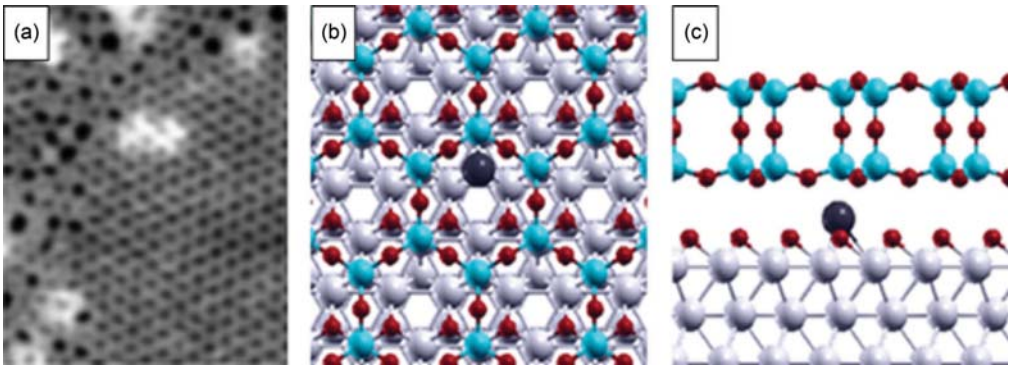

FIG. 2. (Color online) (a) STM image of ~5 × 10^{12} Pd/cm^2 on bilayer SiO_2/Ru(0001) at ~5 K. Image is 10 × 8.4 nm^2, and was taken at constant current, with $V_s = 2$ V and $I_T = 100$ pA. (b) Top and (c) side views of a Pd atom bound at the interface between the bilayer SiO_2 film and the O-covered Ru(0001) substrate. Blue, red, light gray, and dark gray spheres represent Si, O, Ru, and Pd atoms, respectively.

and the resultant model derived from DFT calculations [Figs. 2(b) and 2(c)]. Put briefly, Pd adsorption has been assigned to interfacial Ru sites based on the following criteria: (1) The irregular bright protrusions, which do not appear when imaging pristine films, are assigned to the presence of Pd atoms and show remarkable similarity to those noted in analogous experiments conducted over $SiO_{2.5}$/Mo(112), which possesses the same terminal structure as the crystalline domains of the current system (right portion of STM image) and is known to selectively promote subsurface adsorption of Pd atoms via facile diffusion through the film's regular pattern of small pores [36]. (2) The location and appearance of the Pd features are unaffected by repeated STM scans, indicating a level of stability that would be unexpected for atoms binding above the SiO_2 film. (3) DFT calculations show evidence of only weak interactions between Pd atoms and the SiO_2 film and suggest near barrierless diffusion pathways through pores within both domains of the film. (4) In all cases, optimization results in binding arrangements like that shown in Figs. 1(b) and 1(c), with Pd atoms being stabilized at the SiO_2-Ru interface.

Due to experimental constraints (cryostat cooling limitations and sensitivity requirements), the conditions used to create samples like those shown in Fig. 2(a) could not be identically duplicated for the XPS study. Instead, Fig. 3(a) shows a Pd 3*d* XPS spectrum collected from a sample prepared by dosing bilayer SiO_2/Ru(0001) with ~9 × 10^{13} Pd/cm^2 at 150 K. Relative to the curved background, which is present prior to Pd adsorption, we note three distinct doublet features after fitting the spectrum (we will refer to the $3d_{5/2}$ components when discussing peak positions). The lower BE components at ~334.7 and ~337.1 eV are thought to relate to photoemission from different Pd species on the surface of the sample, whereas the higher BE feature at ~341 eV, which is necessary to properly fit the small peak at ~346 eV, is attributed to electrons leaving the sample after contributing energy to Pd plasmon excitations [37]. Returning to the two primary features, we note that one is shifted below, and the other above, the BE obtained from a Pd(111) reference sample (335.05 eV)—see analogous plot in Fig. 4. The position of the broader peak is qualitatively consistent with shifts commonly reported for small metal clusters supported on insulating materials, where a number of initial- and final-state effects are known to result in positive BE shifts [8,9,38–40], and, because of this, we have tentatively assigned the feature as such. By contrast, the sharper peak shows up at a BE consistent with SCSs from undercoordinated Pd surfaces [5].

To better understand the causes of the XPS shifts, we have additionally measured the Pd $L_3M_{45}M_{45}$ Auger spectrum from the same sample used in Fig. 3(a), and the result of that work is shown in Fig. 3(b). As already mentioned, this plot has been generated after first subtracting the signal recorded from the sample prior to Pd adsorption to remove spurious contributions from weak Ru Auger lines that appear in the same region [41]. To generate the individual fits, we have varied the positions and widths of two peaks whose line shapes and relative intensities are governed by the peak profile obtained from Pd(111) (see Fig. 4) and the ratio of the two primary features in the corresponding XPS spectrum, respectively. Interpretation of the multiplet splitting of these lines is informed by the work of Kleiman *et al.* [42], from which we ascribe the three features (from lower to higher kinetic energy) to transitions with final states within the ^1G and ^3F multiplets.

Unlike the XPS results, both of the corresponding Auger peaks shift in the same direction relative to the KE noted for the single-crystal reference sample (2469.1 eV). Using this data to calculate a modified $\Delta\beta$, we find decreased final-state

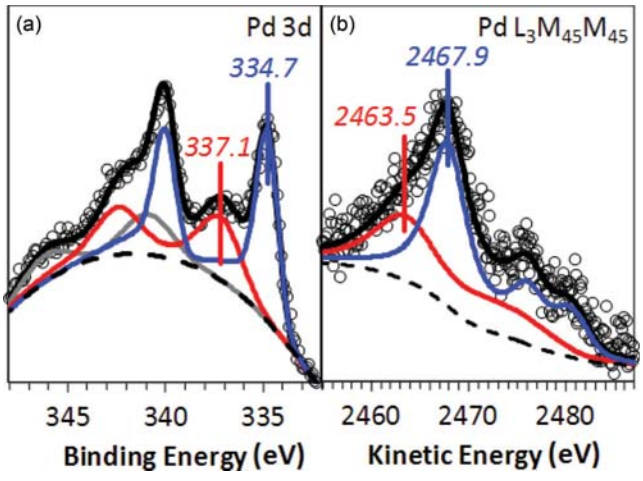

FIG. 3. (Color online) (a) 3*d* XPS and (b) $L_3M_{45}M_{45}$ Auger spectra from ~9 × 10^{13} Pd/cm^2 on bilayer SiO_2/Ru(0001) at ~150 K.

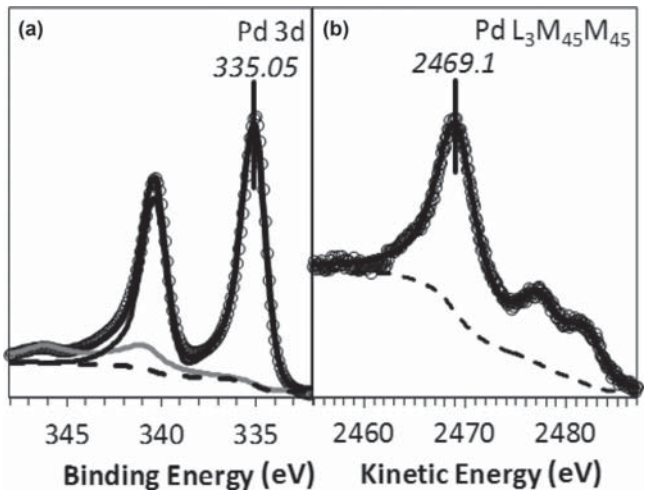

FIG. 4. (a) 3*d* XPS and (b) $L_3M_{45}M_{45}$ Auger spectra from freshly cleaned Pd(111).

screening of the Pd associated with both 3*d* XPS features, relative to that for bulk Pd, which is not unexpected for small supported particles for the variety of reasons that we have already alluded to. Specifically, we note ΔR_{3d} decreases of ~1.8 and ~0.8 eV for the higher and lower BE components, respectively, which imply $\Delta\varepsilon_{3d}$ initial-state changes of roughly −0.3 and +1.1 eV for the Pd associated with those features. (Note: By convention, positive $\Delta\varepsilon$ and ΔR shifts imply negative ΔBE shifts and vice versa.) From this we conclude that the XPS shift associated with the peak ascribed to the presence of SiO_2-supported clusters predominantly reflects the decreased extra-atomic screening from the oxide, while the negative ΔBE associated with the SCS-like feature results from a mixture of competing initial- and final-state effects. Consistent with postulates proposed by Citrin *et al.* [1], the direction of the SCS-like shift is governed by changes to the initial state, while its absolute size is clearly dependent on final-state contributions, in a manner that is consistent with results from the work of Andersen *et al.* [5].

Density functional theory with dispersion corrections (DFT-D2) has been used to generate and investigate model $Pd/SiO_2/Ru(0001)$ systems intended to represent the experimental samples discussed above. Based on the results of these calculations, we find that Pd atoms placed over the samples only bind very weakly to the silica film but may pass through the oxide via nonactivated penetration of the repeating network of vertical pores created by the film's honeycomblike lateral structure. Consistent with our interpretation of the STM image in Fig. 2(a), the Pd atoms may then preferentially bind over unoccupied threefold hollow sites at the SiO_2/Ru interface with an energy of ~3.6 eV [see Figs. 2(b) and 2(c)].

Within the initial-state approximation (Kohn-Sham energy levels), the 3*d* core-level BE for the interface-confined Pd atoms (324.0 eV) is 0.7 eV smaller than that for atoms within bulk Pd (324.7 eV). When final-state effects are included, this shift becomes −0.4 eV; indicating a small relative decrease of 0.3 eV to the relaxation energy contributed to the final state of the supported atoms, which is wholly consistent with the findings of Andersen *et al.*'s investigations into Pd SCSs [5]. For comparison, we provide Fig. 5, which plots these values (in terms of their contribution to the change in Pd 3*d* BE) alongside those obtained from our modified $\Delta\beta$ analysis of the lower BE component in the experimentally obtained XPS spectrum. As can be seen, the calculated ΔBE extracted from the $Pd/SiO_2/Ru(0001)$ model agrees very well with that measured in the experimental system, suggesting that the presence of Ru-bound atoms, like those described in Fig. 2, is likely responsible for the formation of the SCS-like feature in the XPS experiments [Fig. 3(a)].

In addition to very accurately predicting the observed XPS shift, the DFT supercell calculations also show good qualitative agreement with the $\Delta\beta$-extracted initial- and final-state changes. Neglecting the small differences between our experimental and theoretical findings, the negative initial-state core-level shifts (CLSs) noted by both techniques would typically be interpreted as an accumulation of negative charge on the Pd atoms. By contrast, our DFT results indicate that incorporated Pd exhibit a partial positive charge (+0.3 $|e|$), which is consistent with secondary-electron threshold measurements of $SiO_2/Ru(0001)$ samples that show decreased work functions after depositing Pd to create model systems like those described above [35,43,44]. Therefore, our CLSs cannot be straightforwardly attributed to charge-transfer effects via the classical approach. Instead, our CLSs appear to relate to changes in the degree of 4*d*-5*sp* hybridization of Pd as its coordination is varied. Relative to bulk atoms, which are more $4d^9$-$5s^1$-like, less-coordinated atoms, like those binding at the SiO_2-Ru interface (or the surface layer of single crystals), adapt a more $4d^{10}$-like configuration. By altering the distribution of the valence-level electrons, the electrostatic potential at the

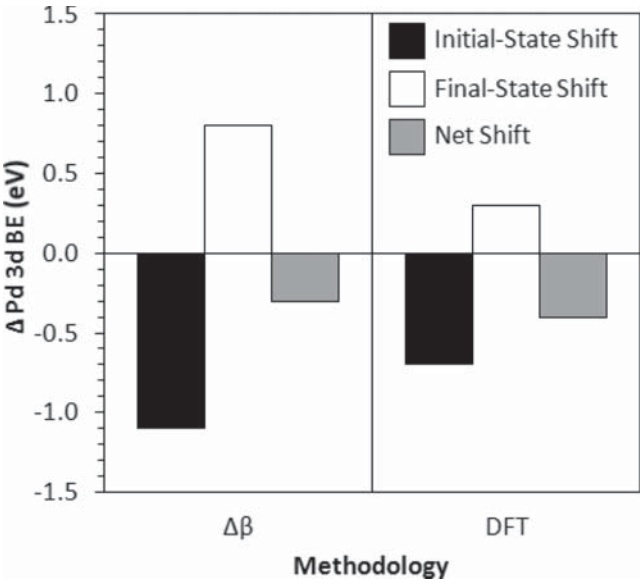

FIG. 5. Experimentally measured changes to the 3*d* BE of the SCS-like Pd ($\Delta\beta$), relative to bulk, are compared to those derived from theoretical calculations (DFT) of the SiO_2/Ru-supported system described by Fig. 2. Included with the total expected/detected shifts (gray) are the partioned contributions attributed to changes in the initial- (black) and final-state (white) configurations of the photoemission process.

TABLE I. Decomposition of the Pd 3*d* BE shifts and other properties between Pd_{13} and Pd_1; see text for definitions of the quantities; energies in eV and $N_P(4d)$ in electrons.

	ΔBE(KT)	ΔBE(R)	ΔBE(ΔSCF)
Direct	+1.96	−2.87	−0.91
$\Delta\beta$	+1.88	−2.79	–
$\Delta\beta^*$	+1.85	−2.75	–
$E(R)$	Pd_1	Pd_{13}	
Auger(*LMM*)	61.48	72.78	
BE(3*d*)	15.71	18.58	
Ratio	3.91	3.92	
$N_P(4d)$	10.0	9.91	

nucleus of these atoms changes in a manner that results in upward core-level orbital-energy shifts (i.e., negative initial-state ΔBEs), which outweigh the decreases in extra-atomic screening and local electron density. This trend between the degree of *d*-*sp* hybridization and initial-state ΔBE is consistent with results from previous theoretical investigations, in which hybridization effects were shown to be of general importance to CLSs [7,32,39,45,46].

Despite the good agreement between the experimental and DFT results, our theoretically derived values appear to slightly underestimate those obtained from the modified $\Delta\beta$ analysis, even when taking the uncertainty associated with the latter values (∼0.3 eV) into account. To test the reliability of the Auger parameter decomposition of the Pd 3*d* BE shifts into initial- and final-state effects, we have also carried out *ab initio* Hartree-Fock (HF) theoretical decompositions of the ΔBEs, like those described in Ref. [32], and provide results from this work in Tables I and II.

In Table I we decompose the 3*d* ΔBE shifts between Pd_{13} and an isolated Pd atom (Pd_1), where the different ΔBEs are defined as $\Delta BE = BE(Pd_{13}) - BE(Pd_1)$. The contributions provided are for the initial-state shift, denoted ΔBE(KT), the final-state relaxation shift, denoted $\Delta BE(R)$, and the total shift, denoted ΔBE(ΔSCF). The relaxation shift for the BE is computed as $\Delta BE(R) = E_R(Pd_1) - E_R(Pd_{13})$ to capture the effect that this difference has on the Pd_{13} BE relative to that for the Pd_1. These shifts are computed in three ways. The first is from direct SCF calculations of the different BEs for Pd_1 and Pd_{13} [32]. The second is from the β Auger parameter using the HF calculated values for Pd 2*p* and 3*d* BEs and the *LMM* Auger states; see Eq. (7). The third is from the Auger parameter obtained with the Pd 3*d* BE and the *LMM* Auger states denoted β^*; see Eq. (8). In the table we also include the directly calculated HF relaxation energies (E_R) for the single, BE(3*d*), and double, Auger (*LMM*), 3*d*-hole configurations for Pd_1 and Pd_{13}. In addition, we also provide the Pd 4*d* occupation, $N_P(4d)$, obtained by projection [32,47]. In Table II we give the same information for a comparison of the Pd/Ru_9 and Pd_{13} clusters, which were intended to provide crude approximations of the supported and bulk samples discussed above.

TABLE II. Decomposition of the Pd 3*d* BE shifts and other properties between Ru_9Pd and Pd_{13}; see text for definitions of the quantities; energies in eV and $N_P(4d)$ in electrons.

	ΔBE(KT)	ΔBE(R)	ΔBE(ΔSCF)
Direct	+0.18	−0.04	+0.14
$\Delta\beta$	+0.22	−0.08	–
$\Delta\beta^*$	+0.25	−0.11	–
$E(R)$	Pd_{13}	Ru_9Pd	
Auger(*LMM*)	72.78	73.03	
BE(3*d*)	18.58	18.62	
Ratio	3.92	3.92	
$N_P(4d)$	9.91	9.89	

In both cases, the decomposition of the total ΔBE(ΔSCF) by the Auger parameter analysis is rather similar to the directly computed decompositions with, for the more approximate $\Delta\beta^*$ analysis, errors that are ∼0.1 eV. This is a strong justification for the reliability of the modified Auger parameter analysis and suggests that some of the discrepancy between the experimental and DFT values plotted in Fig. 5 might result from approximations inherent to the level of theory needed to make the realistic calculations of this fairly complicated system. In part, this reliability arises because the ratio of the relaxation energy associated with the single-hole photoelectron and the double-hole Auger final states is very close to 4 in all cases, which shows good agreement with the approximation made in Eq. (4).

In the more bulklike Pd_{13} cluster, the central atom has ∼0.1 electron hybridized from 4*d* to 5*sp* to contribute to the formation of Pd-Pd bonds [15]. Consistent with the DFT analysis, it is this hybridization that leads to a ∼2 eV increase of the 3*d* BE(KT) for Pd_{13} relative to the isolated atom (Table I). However, the extra-atomic relaxation present for Pd_{13}, but absent in the isolated atom, reduces the 3*d* BE by ∼3 eV, which leads to a net lowering of the Pd_{13} BE by ∼1 eV. These trends are entirely consistent with those observed for Pd atoms when confined to the SiO_2/Ru(0001) interface vs

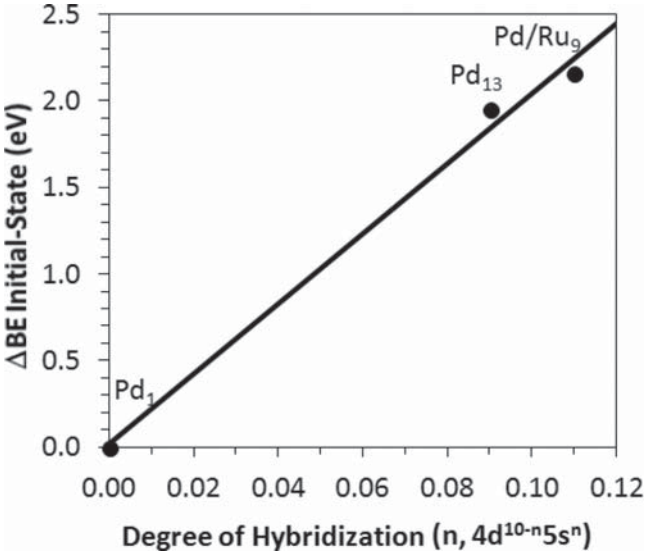

FIG. 6. Initial-state shifts (vs Pd_1) to the Pd 3*d* BEs are plotted relative to the degree of 4*d*-5*sp* hybridization for the Pd_1, Pd_{13}, and Pd/Ru_9 clusters depicted in Fig. 1.

the bulk metal. That the absolute size of the shifts exceeds those of the samples explored in the main text is not surprising since an atom in contact with a metal surface is expected to be more hybridized and better screened than an isolated atom. While the Pd/Ru_9 cluster appears to be too simple to reproduce the physics of the supported samples discussed above, we do note a continued correlation between the degree of hybridization and the resultant initial-state ΔBE for the Pd atoms as a function of environment when comparing this cluster to Pd_{13} (Table II). To exemplify this trend, we include Fig. 6, which plots the change in initial-state BE as a function of the degree of *d*-*sp* hybridization for Pd in each of the cluster models. As the degree of hybridization in our $Pd/SiO_2/Ru$ DFT models was determined to be less than that for bulk Pd, our negative ΔBE initial-state shifts are exactly what this plot would predict.

V. CONCLUSION

To our knowledge, these results represent the first time that a properly vetted Auger parameter analysis has been used to experimentally validate the conclusions drawn from a theoretical investigation of the driving forces governing SCSs in XPS. Such evidence puts our theoretical interpretation, which asserts that large initial-state effects resulting from decreased 4*d*-5*sp* hybridization in surface vs bulk Pd atoms outweigh counterbalancing charge transfer and final-state screening effects to yield net-negative ΔBEs, on a stronger foundation than those put forth in previous works. In addition, this work helps to further substantiate (or detract from) some of the theories put forward in several previous works, where similar (or contradictory) claims have been made [4,5,45].

ACKNOWLEDGMENTS

W.E.K. acknowledges the Alexander von Humboldt Foundation for their financial support of this work. F.R. and M.S. acknowledge support from the European Reasearch Council for project number 280070 within the FP7-IDEAS-ERC program. L.V. and G.P. would like to acknowledge financial support from the Italian MIUR through the Project RBAP115AYN "Oxides at the nanoscale: multifunctionality and applications." P.S.B. acknowledges support by the Geosciences Research Program, Office of Basic Energy Sciences, US DOE.

[1] P. H. Citrin, G. K. Wertheim, and Y. Baer, Phys. Rev. Lett. **41**, 1425 (1978).
[2] T. M. Duc, C. Guillot, Y. Lassailly, J. Lecante, Y. Jugnet, and J. C. Vedrine, Phys. Rev. Lett. **43**, 789 (1979).
[3] P. H. Citrin, G. K. Wertheim, and Y. Baer, Phys. Rev. B **27**, 3160 (1983).
[4] P. H. Citrin and G. K. Wertheim, Phys. Rev. B **27**, 3176 (1983).
[5] J. N. Andersen, D. Hennig, E. Lundgren, M. Methfessel, R. Nyholm, and M. Scheffler, Phys. Rev. B **50**, 17525 (1994).
[6] B. Johansson and N. Mårtensson, Phys. Rev. B **21**, 4427 (1980).
[7] P. S. Bagus, A. Wieckowski, and H.-J. Freund, Comput. Theor. Chem. **987**, 22 (2012).
[8] G. K. Wertheim, S. B. DiCenzo, and S. E. Youngquist, Phys. Rev. Lett. **51**, 2310 (1983).
[9] C. C. Chusuei, X. Lai, K. Luo, and D. W. Goodman, Top. Catal. **14**, 71 (2001).
[10] C. D. Wagner, Faraday Discuss. Chem. Soc. **60**, 291 (1975).
[11] C. D. Wagner and A. Joshi, J. Electron Spectrosc. Relat. Phenom. **47**, 283 (1988).
[12] C. D. Wagner and J. A. Taylor, J. Electron Spectrosc. Relat. Phenom. **28**, 211 (1982).
[13] G. Hohlneicher, H. Pulm, and H.-J. Freund, J. Electron Spectrosc. Relat. Phenom. **37**, 209 (1985).
[14] R. N. Sodhi and R. G. Cavell, J. Electron Spectrosc. Relat. Phenom. **32**, 283 (1983).
[15] P. S. Bagus, A. Wieckowski, and H.-J. Freund, Chem. Phys. Lett. **420**, 42 (2006).
[16] B. Yang, W. E. Kaden, X. Yu, J. A. Boscoboinik, Y. Martynova, L. Lichtenstein, M. Heyde, M. Sterrer, R. Włodarczyk, M. Sierka, J. Sauer, S. Shaikhutdinov, and H.-J. Freund, Phys. Chem. Chem. Phys. **14**, 11344 (2012).
[17] L. Lichtenstein, M. Heyde, and H.-J. Freund, Phys. Rev. Lett. **109**, 106101 (2012).
[18] R. Wlodarczyk, M. Sierka, J. Sauer, D. Löffler, J. J. Uhlrich, X. Yu, B. Yang, I. M. N. Groot, S. Shaikhutdinov, and H.-J. Freund, Phys. Rev. B **85**, 085403 (2012).
[19] L. Lichtenstein, C. Büchner, B. Yang, S. Shaikhutdinov, M. Heyde, M. Sierka, R. Wlodarczyk, J. Sauer, and H.-J. Freund, Angew. Chem., Int. Ed. **51**, 404 (2012).
[20] H.-P. Rust, T. König, G. H. Simon, M. Nowicki, V. Simic-Milosevic, G. Thielsch, M. Heyde, and H.-J. Freund, Rev. Sci. Instrum. **80**, 113705 (2009).
[21] C. J. Powell and A. Jablonski, NIST Standard Reference Database (2011), http://www.nist.gov/srd/upload/SRD82UsersGuideV1-3.pdf.
[22] H. Pulm, G. Hohlneicher, H.-J. Freund, H. U. Schuster, J. Drews, and U. Eberz, J. Less Common Metals **115**, 127 (1986).
[23] G. Kresse and J. Hafner, Phys. Rev. B **47**, 558 (1993).
[24] G. Kresse and J. Furthmüller, Phys. Rev. B **54**, 11169 (1996).
[25] P. E. Blöchl, Phys. Rev. B **50**, 17953 (1994).
[26] J. P. Perdew, K. Burke, and M. Ernzerhof, Phys. Rev. Lett. **77**, 3865 (1996).
[27] S. J. Grimme, Comput. Chem. **27**, 1787 (2006).
[28] R. F. W. Bader, Chem. Rev. **91**, 983 (1991).
[29] L. Köhler and G. Kresse, Phys Rev B **70**, 165405 (2004).
[30] R. W. G. Wyckoff, *Crystal Structures* (Wiley, New York, 1963).
[31] L. Visscher, O. Visser, P. J. C. Aerts, H. Merenga, and W. C. Nieuwpoort, Comput. Phys. Commun. **81**, 120 (1994).
[32] P. S. Bagus, E. S. Ilton, and C. J. Nelin, Surf. Sci. Rep. **68**, 273 (2013).
[33] P. J. Hay and W. R. Wadt, J. Chem. Phys. **82**, 299 (1985).
[34] R. Ahlrichs and K. May, Phys. Chem. Chem. Phys. **2**, 943 (2000).
[35] C. Büchner, W. E. Kaden, L. Lichtenstein, S. Stuckenholz, F. Ringleb, M. Sterrer, M. Heyde, L. Giordano, G. Pacchioni, and H.-J. Freund (unpublished).

[36] S. Ulrich, N. Nilius, H.-J. Freund, U. Martinez, L. Giordano, and G. Pacchioni, Surf. Sci. **603**, 1145 (2009).
[37] F. P. Netzer and M. M. El Gomati, Surf. Sci. **124**, 26 (1983).
[38] W. E. Kaden, T. Wu, W. A. Kunkel, and S. L. Anderson, Science **326**, 826 (2009).
[39] B. Richter, H. Kuhlenbeck, H.-J. Freund, and P. S. Bagus, Phys. Rev. Lett. **93**, 026805 (2004).
[40] M. D. Kane, F. S. Roberts, and S. L. Anderson, Faraday Discuss. Chem. Soc. **162**, 323 (2013).
[41] K. D. Childs, B. A. Carlson, L. A. LaVanier, J. F. Moulder, D. F. Paul, W. F. Stickle, and D. G. Watson, *Handbook of Auger Electron Spectroscopy*, 3rd ed. (Physical Electronics, Prairie, Mn, 1995).
[42] G. G. Kleiman, R. Landers, S. G. C. de Castro, and A. de Siervo, Phys. Rev. B **58**, 16103 (1998).
[43] K. H. Kingdom and I. Langmuir, Phys. Rev. **21**, 380 (1923).
[44] R. W. Gurney, Phys. Rev. **47**, 479 (1935).
[45] P. S. Bagus and G. Pacchioni, Phys. Rev. B **48**, 15274 (1993).
[46] P. S. Bagus, G. Pacchioni, and F. Parmigiani, Phys. Rev. B **43**, 5172 (1991).
[47] C. J. Nelin, E. S. Ilton, and P. S. Bagus, J. Chem. Phys. (unpublished).